

2004 NOAA ICARTT/NEAQS
Field Program on the NOAA Ship Ronald H. Brown
July 6 – August 12, 2004
Results from the ETL Cloud and Flux Group and University of Miami Measurements

C. W. Fairall, J. Hare, D. Wolfe, Michelle Ratteree, Dan Law, Tom Snowden and Ieng Jo
NOAA Environmental Technology Laboratory
Boulder, CO USA
August 12, 2004

1. Background on Measurement Systems

The ETL air-sea flux and cloud group conducted measurements of fluxes and near-surface bulk meteorology during the summer field program of air quality studies off the coast of New England at 40-45 N Latitude 69-74 W Longitude. The air-sea flux system consists of six components. (1) A fast turbulence system with ship motion corrections mounted on the jackstaff. The jackstaff sensors are: INUSA Sonic anemometer, OPHIR IR-2000 IR-hygrometer, LiCor LI-7500 fast CO₂/hygrometer, and a Systron-Donner motion-pak. (2) A mean T/RH sensor in an aspirator on the jackstaff. (3) Solar and IR radiometers (Eppley pyranometers and pyrgeometer) mounted on top of a mast in front of 02 deck. (4) A near surface sea surface temperature sensor consisting of a floating thermistor deployed off port side with outrigger. (5) An optical rain gauge mounted on the bow tower. (6) A Riegl lidar range finder mounted on the bow used to measure surface gravity wave displacements of the sea surface. Slow mean data (T/RH, PIR/PSP, etc) are digitized on Campbell 21x datalogger and transmitted via RS-232 as 1-minute averages. A central data acquisition computer logs all sources of data via RS-232 digital transmission:

1. Sonic Anemometer
2. Licor CO₂/H₂O
3. Slow means (Campbell 21x)
4. Laser wave gauge
5. OPHIR hygrometer
6. Systron-Donner Motion-Pak
7. Ship's SCS
8. ETL GPS

The 8 data sources are archived at full time resolution. At sea we run a set of programs each day for preliminary data analysis and quality control. As part of this process, we produce a quick-look ascii file that is a summary of fluxes and means. The data in this file come from three sources: The ETL sonic anemometer (acquired at 21.3 Hz), the ships SCS system (acquired at 2 sec intervals), and the ETL mean measurement systems (sampled at 10 sec and averaged to 1 min). The sonic is 5 channels of data; the SCS file is 15 channels, and the ETL mean system is 42 channels. A series of programs are run that read these data files, decode them, and write daily text files at 1 min time resolution. A second set of programs reads the daily 1-min text files, time matches the three data sources, averages them to 5 or 30 minutes, computes fluxes, and writes new daily flux files. The 5-min daily flux files have been combined and rewritten as a single file

to form the file *flux_5hf_neaqs_04.txt*. The 1-min daily ascii files are stored as *proc_nam_dayDDD.txt* (nam='pc', 'scs', or 'son'; DDD=yearday where 000 GMT January 1, 2004 =1.00). File structure is described in the original matlab files that write the data, *prt_nam_03.m*.

ETL/Flux and UM also operated five remote systems: a Vaisala CT-25K cloud base ceilometer, a 94 GHz vertically pointed Doppler cloud radar, a 20.6-31.65 GHz microwave radiometer, a 60 GHz scanning microwave radiometer, and the RHB's scanning Doppler C-band radar.. The ceilometer is a vertically pointing lidar that determines the height of cloud bottoms from time-of-flight of the backscatter return from the cloud. The time resolution is 30 seconds and the vertical resolution is 15 m. The raw backscatter profile and cloud base height information deduced from the instrument's internal algorithm are stored in daily files with the naming convention *CRVYYDDD.raw* where YY=04 and DDD=julian day. File structure is described in *ceilo_readme.txt*.

ETL/Flux and UM used an integrated system in a seatainer that includes a Doppler W-band cloud radar (UMWBR) and the 2-channel microwave radiometer. The system can be used to deduce profiles of cloud droplet size, number concentration, liquid water concentration etc. in stratus clouds. If drizzle (i.e., droplets of radius greater than about 50 μm) is present in significant amounts, then the microphysical properties of the drizzle can be obtained from the first three moments of the Doppler spectrum. The radar is extremely sensitive and can detect most cirrus and fair weather cumulus clouds. The Doppler capability can also be used to measure in-cloud vertical velocity statistics. The scanning 60-GHz microwave radiometer data will be used to retrieve continuous profiles of temperature in the lowest 200 m. The C-band radar was operated continuously with a scan sequence program consisting of alternating a 0.5 deg elevation survey scan with a multiple elevation angle volume scan.

2. Selected Samples

a. Flux Data

Preliminary flux data is shown for yearday=223 (August 10, 2004); the cruise track is shown in Fig. 1. The time series of ocean and air temperature is given in Fig. 2. The water temperature is about 18 C and the air temperature varies from about 18 to 24 C. Wind direction (Fig. 3) changed from south westerly to southerly during the day while the wind speed (Fig. 4) increased from 5 to 10 m/s. The effect of a few scattered clouds on the downward solar flux is seen in Fig. 5 and on the IR flux in Fig. 6. For the solar flux, broken clouds are apparent in the spikes in the curve ; upward spikes are usually caused by reflections from clouds. For IR flux, clear skies have values of about 320 Wm^{-2} and low overcast cloudy skies values around 400 Wm^{-2} . The significant event at 1800 GMT is a fog bank. Fig. 7 shows the time series of four of the five primary components of the surface heat balance of the ocean (solar flux is left out). On this clear day, the largest term is the net IR flux (downward minus upward), followed by the latent heat (evaporation) flux, the sensible heat flux, and the flux carried by precipitation (0 because there is no precipitation). We are using the meteorological sign convention for the turbulent fluxes so a positive sensible or latent flux cools the interface. A negative sensible heat flux (water cooler than air) implies a stably stratified boundary layer; this condition occurred about 80% of the time during the experiment. The time series of net heat flux to the ocean is shown in

Fig. 8. The sum of the components in Fig. 7 is about -60 Wm^{-2} , which can be seen in the night time values in Fig. 8; the large positive peak during the day is due to the solar flux.. The integral over the entire day gives an average flux of 201 Wm^{-2} , indicating strong warming of the ocean mixed layer

b. Remote Sensing Data

A sample ceilometer 24-hr time-height cross section for August 1 is shown in Fig. 9 and the cloud-base heights in Fig. 10 (we chose August 1 rather than August 10 because the clouds were more interesting). This figure shows color-coded backscatter intensity. This day had 26% cloud cover and several sets of cloud base heights: a broken stratus layer with cloud bases 3000 to 4000 m, a cirrus layer at 6500 to 10000 m, and occasional lower level ‘scud’ clouds with bases about 500 m. Precipitation can be seen as the bright color right below cloud base (e.g., 1200 and 1800 GMT). An aerosol scattering layer is also visible as the lighter shading below about 500 m at the beginning of the image; the layer decreases to about 250 m thick by the end. A sample time-height cross section of backscatter intensity (Fig. 11) from the cloud radar is shown for a 24-hr period on August 1. This happens to be a day with a frontal precipitation event between 1200 and 1800; intense precipitation occurred at 1800. Light drizzle events are apparent between 1200 and 1500; the radar is much more sensitive to drizzle than the ceilometer. This drizzle apparently did not reach the surface.

The scanning C-band (5 cm wavelength) Doppler radar ran continuously recording large volumes of data. One sample (Fig. 12) of the low elevation survey scan is shown for 1030 GMT on August 1. The front approaching from the southwest is apparent as the near linear feature in the lower left quadrant. The threshold in this image (2 dBZ) is very light drizzle. This front lost coherence quickly but led to precipitation later in the day. This radar is principally intended to measure precipitation and wind structures in precipitating systems. It is also sensitive enough to make boundary layer wind profile measurements (VAD method) in all conditions.

A simple time-height cross section from the wind profiler is shown (Fig. 13) for August 2 (August 1 had less data because of interference from the Appledore Island wind profiler). The winds are shown as a standard meteorological wind bard plot (time going right to left). Winds aloft are predominately from the west; the lower level winds start out westerly but rotate to southerly then easterly. The wind profiler operates at 33 cm wavelength where it is sensitive enough to detect returns from turbulent variations in radar refractive index, principally associated with atmospheric moisture; it also sensitive to precipitation. Both of these factors cause improved height performance in stormy conditions.

3. Cruise Summary Results

a. Basic Time Series

The cruise track for the entire cruise (both legs) is shown in Fig. 14. The 5-min time resolution time series for sea/air temperature are shown in Fig. 15 and for wind speed and N/E components in Fig.16. The ocean temperature measurements are principally associated with movement of the ship; the cold excursions occurred during visits to the northern end of the domain. Air-sea temperature difference is usually small over the open ocean; here large

differences usually occur near the coast where fetch is too short for the air temperature to adjust from the land boundary layer. The wind variations are dominated by synoptic variability with weak frontal passages and strong southerly winds every 4 days. Fig. 17 gives the surface heat flux components, which are dominated by solar heating. The large positive values on sensible heat flux on day 222 are misleading because the ship is docked in Boston. Fig. 18 shows the cloud radiative forcing ($CF = \text{mean flux} - \text{clear sky flux}$) and the daily precipitation. CF is a good indicator of synoptic disturbance because of the associated low clouds and rain. Thus, Fig. 18 clearly shows the 4-day cycle of disturbances (note, days 205-207 are missing during the import in Portsmouth, NH). It appears that the strength of the synoptic disturbances was decreasing throughout the experiment.

We have computed a few other cruise-average quantities for general interest. Fig. 19 shows the diurnal average of the N and E wind components. The mean flow is SSW but there is a diurnal cycle with peak-to-peak variations of 3 m/s for the southerly component and 1 m/s for the easterly component. The phase (peaks about 4 am and pm local time) is consistent with a land-sea breeze interaction. The sea surface temperature (Fig. 20) shows coldest water to the NE part of the domain. The air-sea temperature difference (Fig. 21) has strong maxima near the coast, presumably the strong influence of warm land-generated boundary layers under westerly winds. The very warm air over cool water near the coast has the effect of suppressing turbulent transfers. For example, a contour map of ozone deposition velocity (Fig. 22) shows corresponding lower values near the coast.

b. Boundary Layer and Cloud Properties

Beginning on July 6 and ending on August 12 we completed 125 successful rawinsonde launches (4 times daily at 0, 6, 12, and 18 UTC). An additional sonde (ozone) was done on most days by the NASA group. A time-height color contour plot of wind direction for Leg I is shown in Fig. 23; the lower panel shows the relative humidity. Note that easterly winds tend to be shallow (the deepest in this period are about 3 km on 14 July). The high near-surface relative humidities (e.g., July 9, 15, 20) are associated with very low cloud base heights (Fig. 24).

4. ETL Data Cruise Archive

Selected data products and some raw data were made available at the end of the cruise for the joint cruise archive. Some systems (radar, turbulence, microwave radiometer) generate too extravagantly to be practical to share. Compared to processed information, the raw data is of little use for most people. For the cloud radar and the C-band radar we have made available image files only; full digital data will be available later from the ETL website. For the microwave radiometer, the time series after some processing and averaging. No direct turbulent flux information is provided; that will be available after processing is done back in Boulder. However, bulk fluxes are available in the flux summary file. The 60 GHz radiometer does not have realtime processing so no data are provided.

Data Archive Directories

Ceilo	Ceilometer files (processed file, images)
Flux	Air-sea flux files (processed flux files: daily files, cruise file, some m-files)
Sondes	Rawindsonde files (.PTU and .WIND)
Microwv	Microwave radiometer files (processed files; graphic display)
Radar	Image files from cloud radar
Reports	Documentation (cruise report, school writeup, summary image files)

Contact:

C. Fairall

NOAA Environmental Technology Laboratory

325 Broadway

Boulder, CO USA

303-497-3253

chris.fairall@noaa.gov

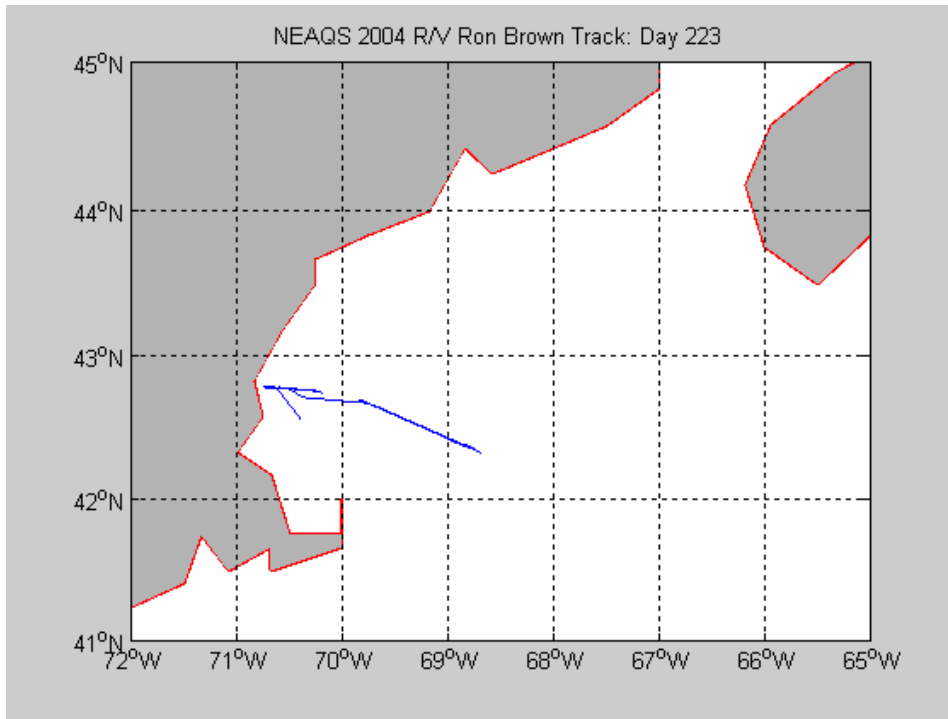


Figure 1. Cruise track for RBH on August 10 (DOY 223).

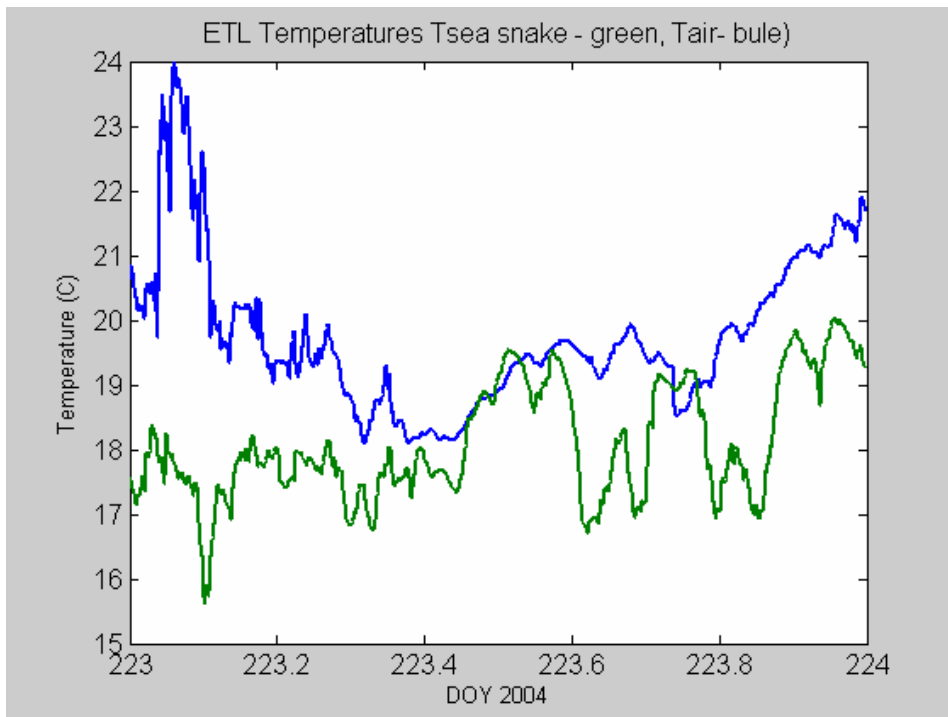


Figure 2. Time series of near-surface ocean temperature and 15-m air temperature.

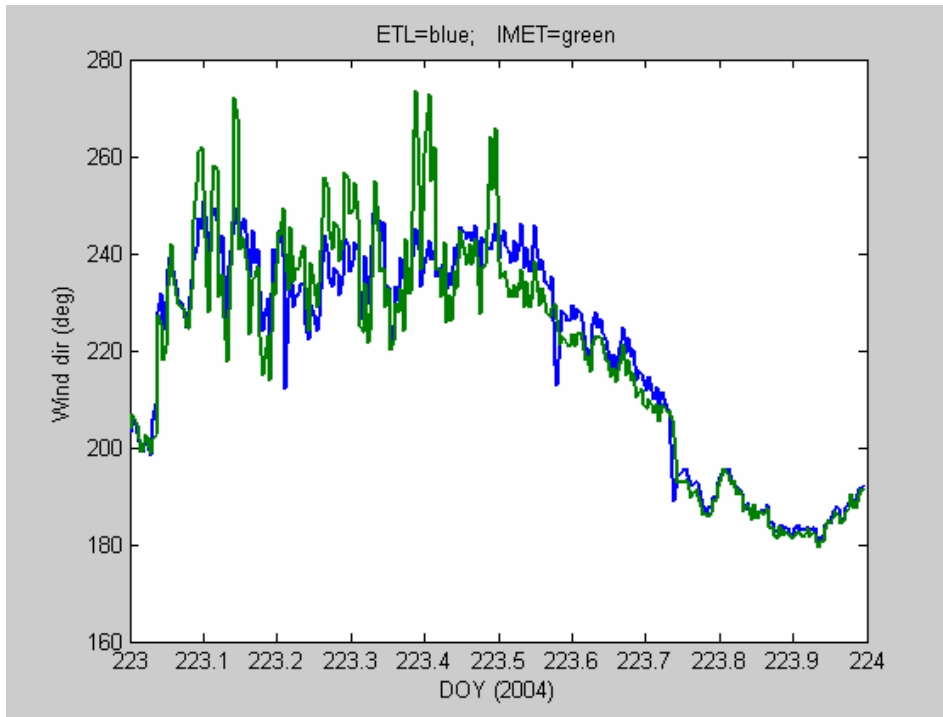


Figure 3. True wind direction from the ETL sonic anemometer (18 m) and the IMET propvane (16 m).

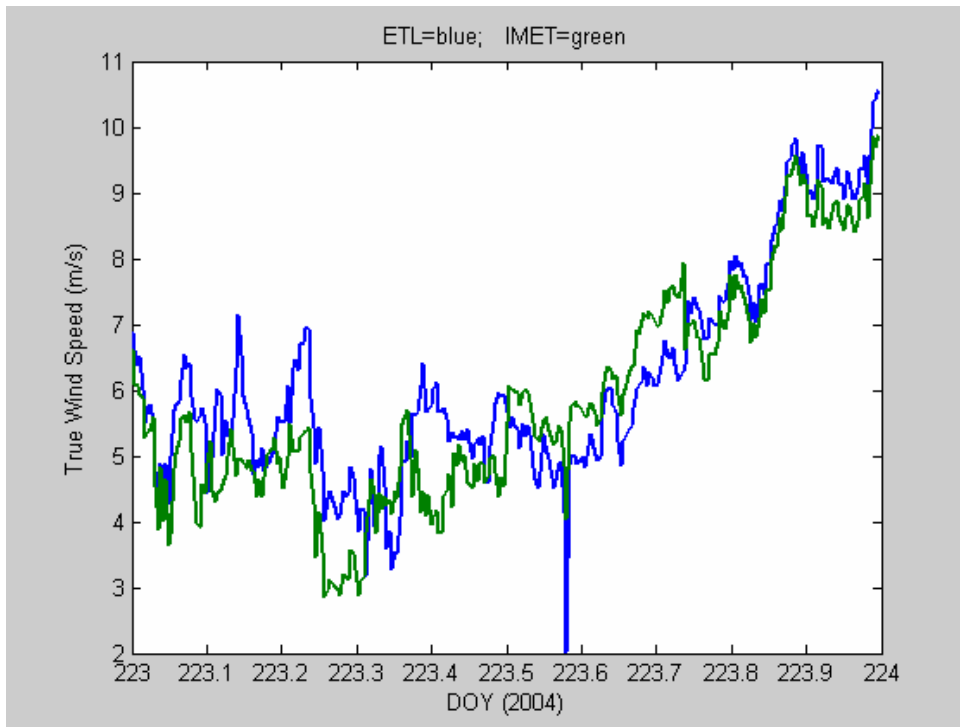


Figure 4. True wind speed from the ETL sonic anemometer (18 m) and the ship's propvane (16 m).

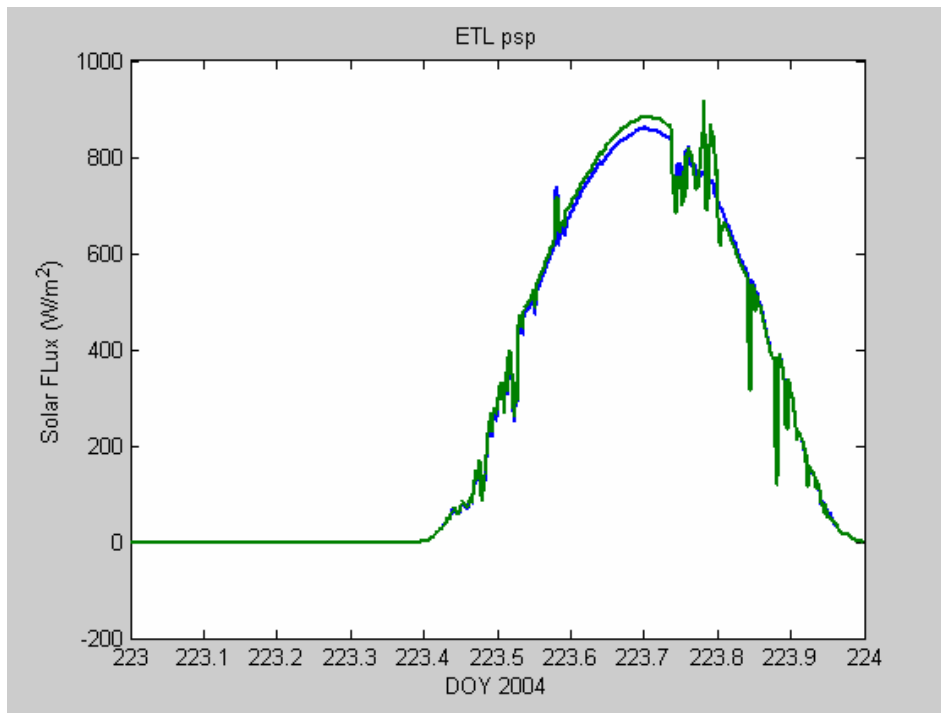


Figure 5. Time series of downward solar flux from two ETL sensors.

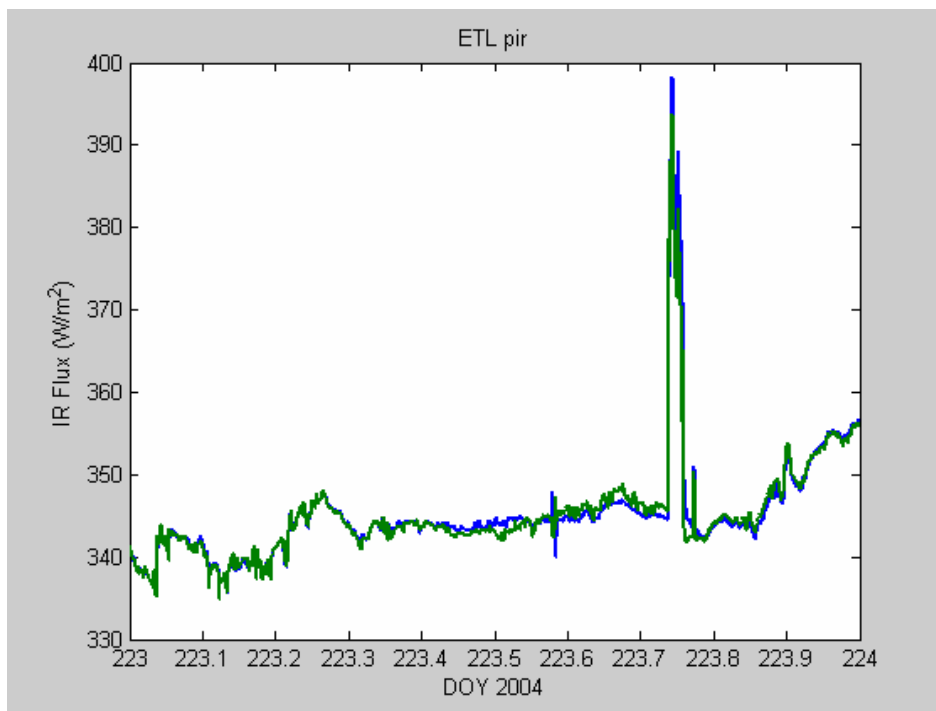


Figure 6. Time series of downward IR flux from two ETL sensors.

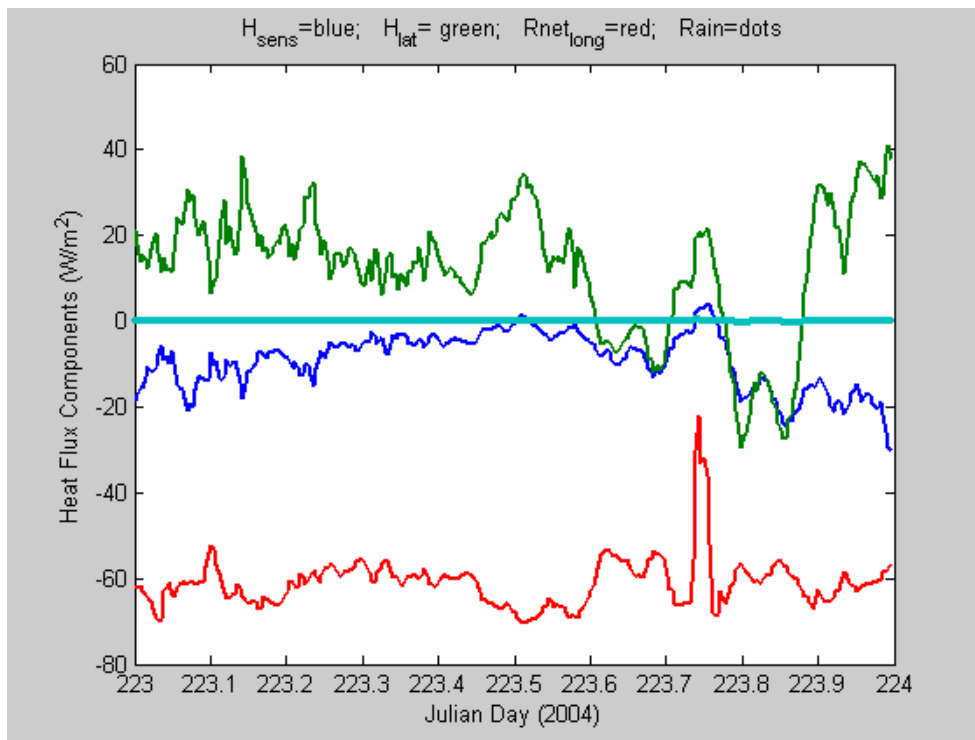


Figure 7. Time series of non-solar surface heat flux components: sensible (blue), latent (green), and net IR (red).

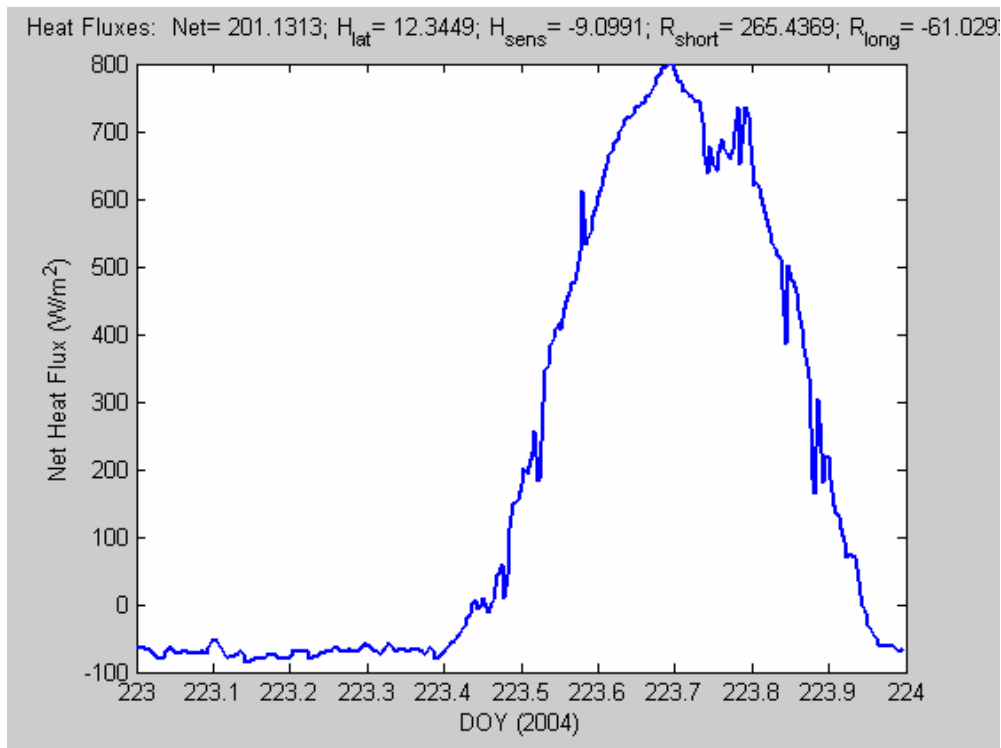


Figure 8. Time series of net heat flux to the ocean surface. The values at the top of the graph are the average for the day.

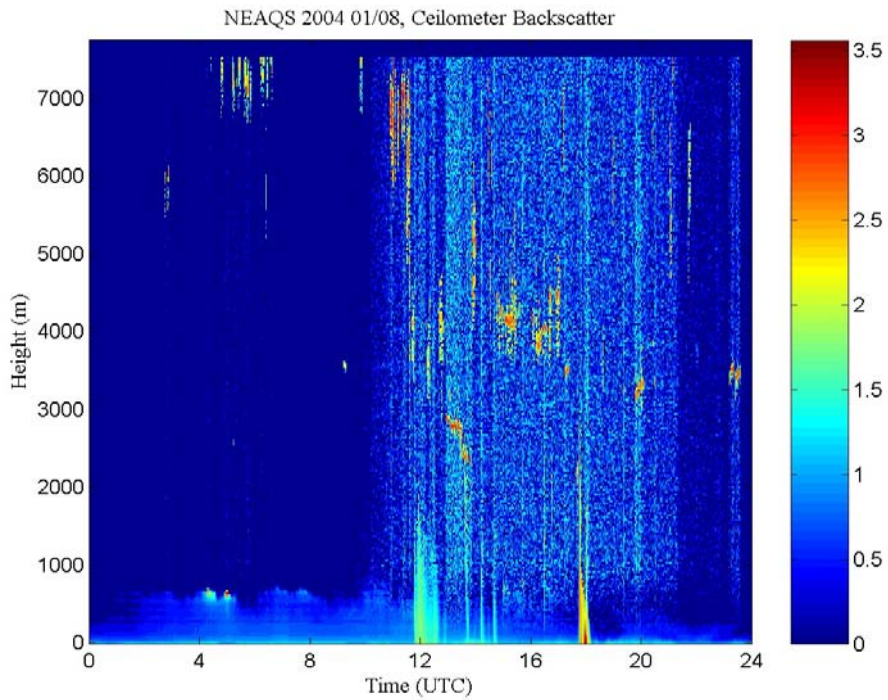


Figure 9. Time height cross-section of low cloud base data for day 214 (August 1, 2004). The colors denote the intensity of the lidar return. The speckled color regions above the clouds are noise caused by diffuse sunlight.

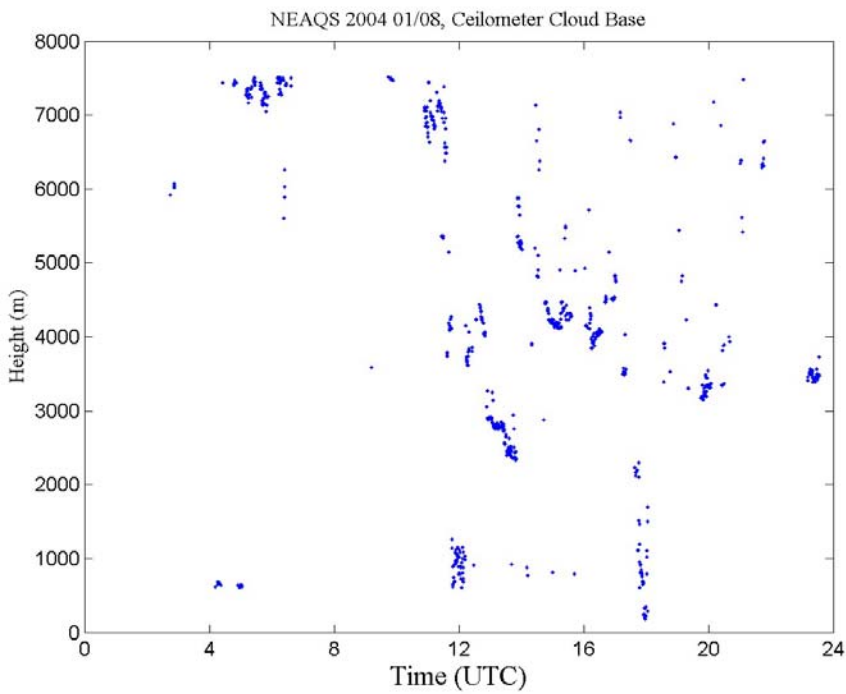


Figure 10. Cloud-base height information extracted from the backscatter data.

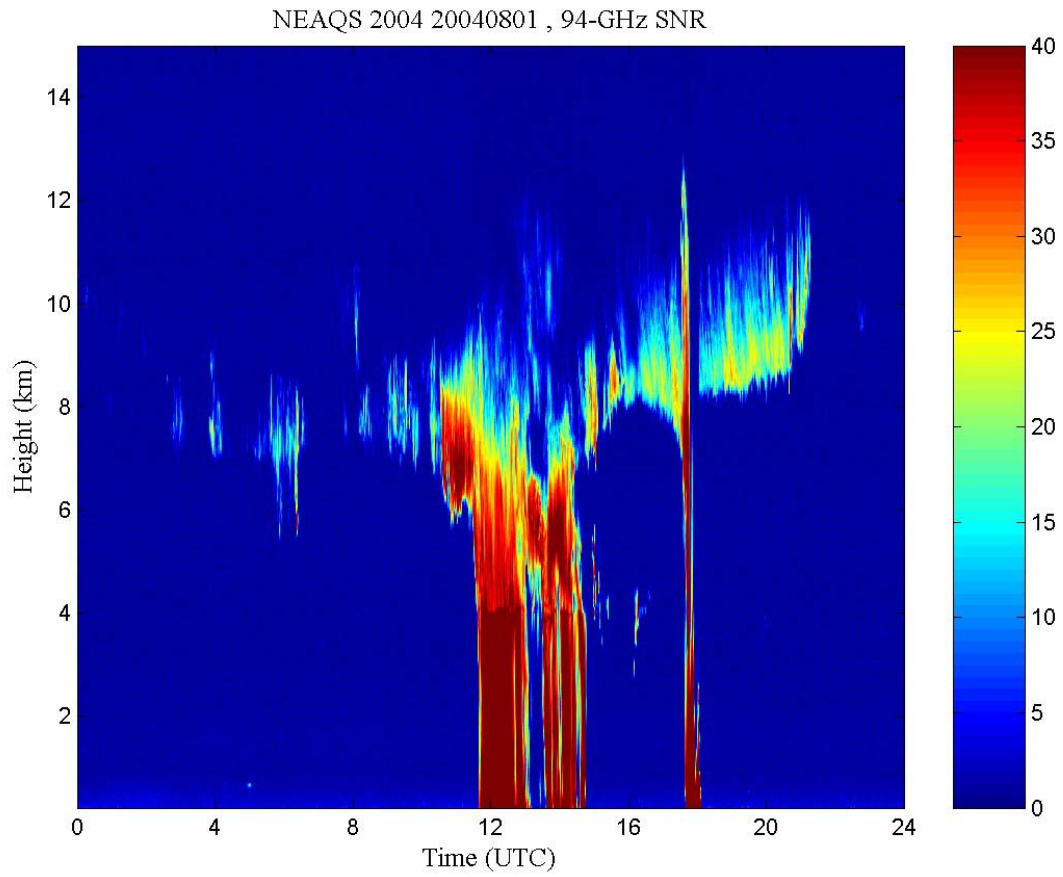


Figure 11. Time-height cross section data from 94 GHz cloud radar backscatter intensity for day 214 (August 1, 2004) . The deep vertical streaks are precipitation.

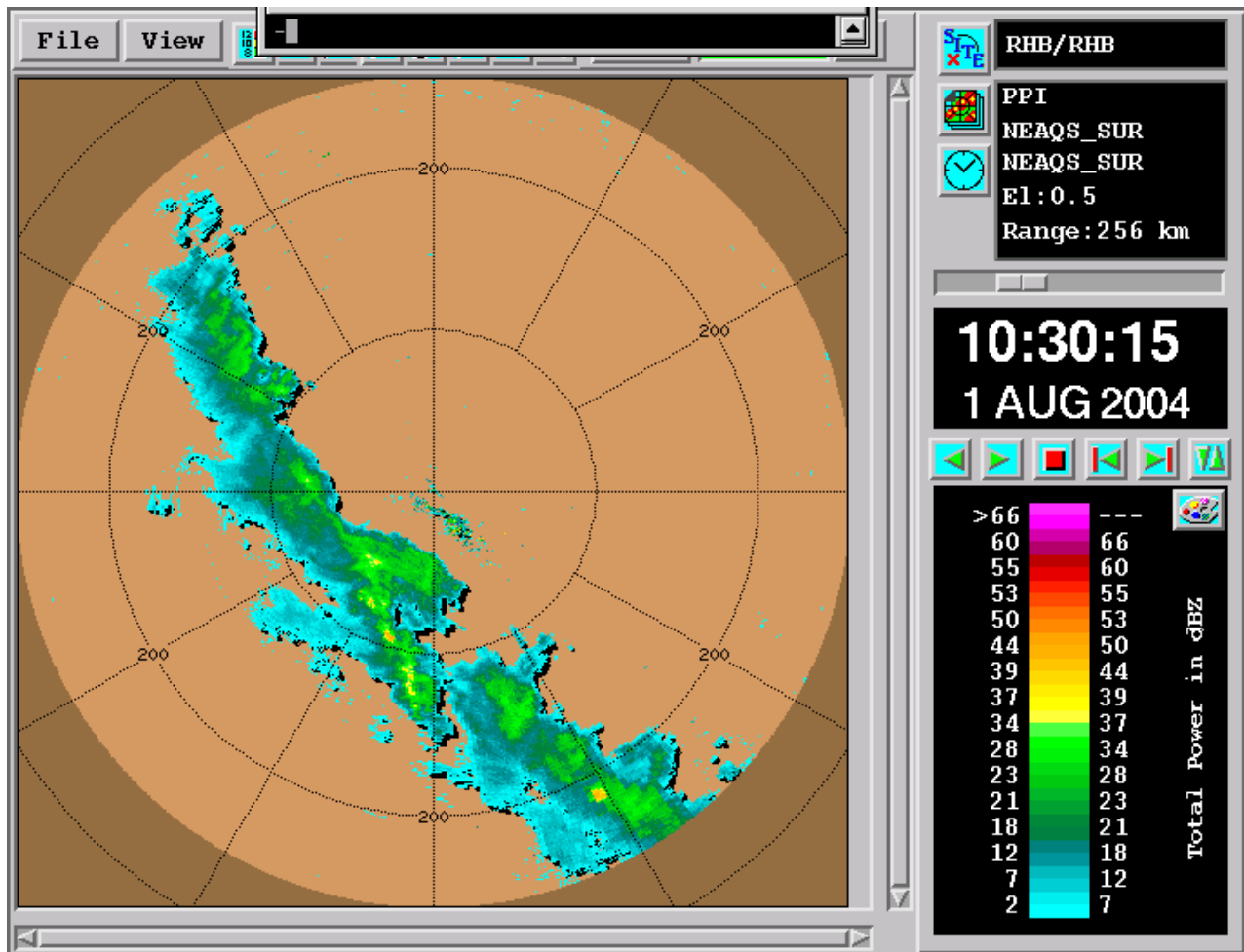


Figure 12. Backscatter intensity image from survey scan of the RHB Doppler C-band radar. Display is in radar dBZ; range rings are in km.

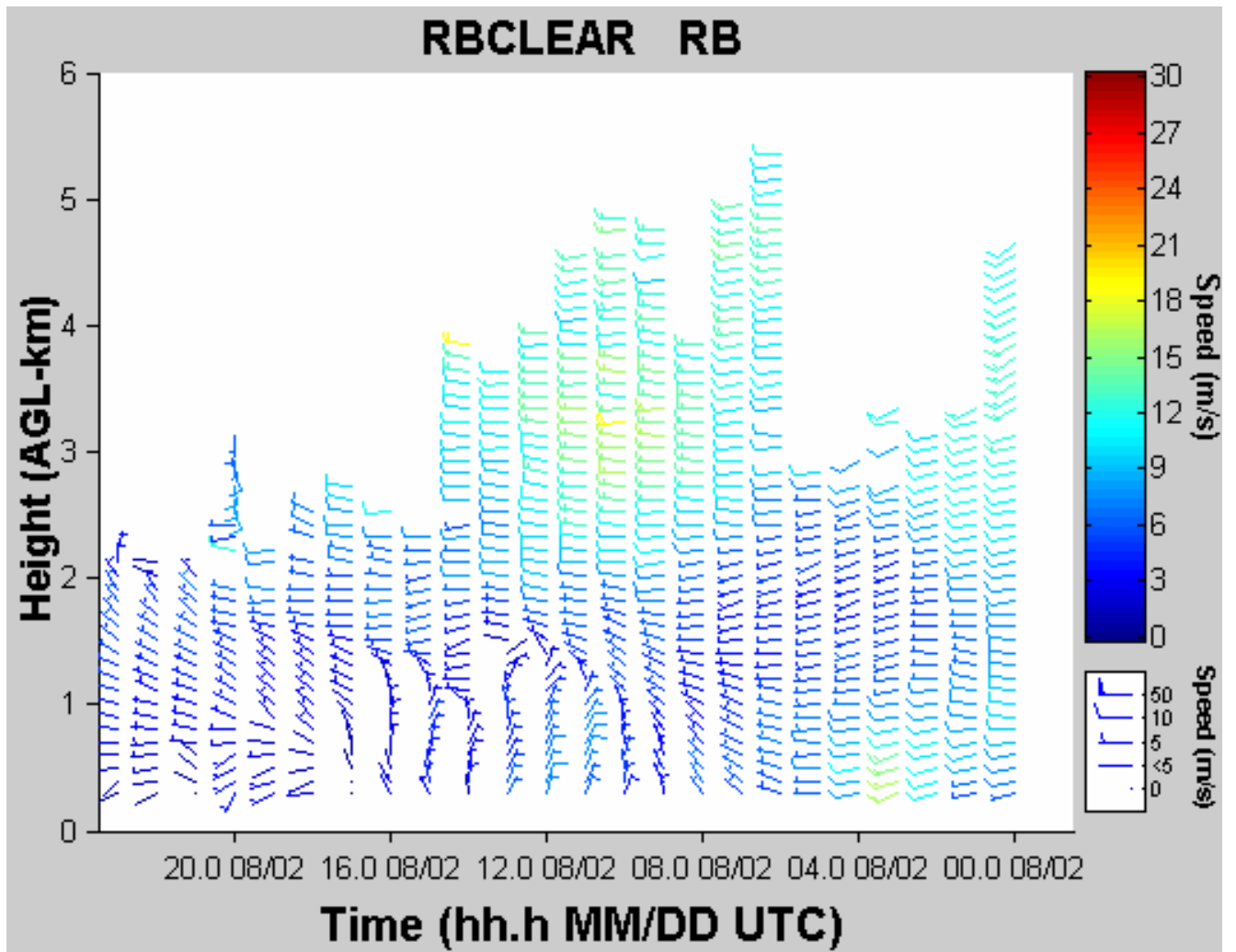


Figure 13. Time-height cross section of wind speed and direction for August 2. Barb orientation gives wind direction; color gives wind speed.

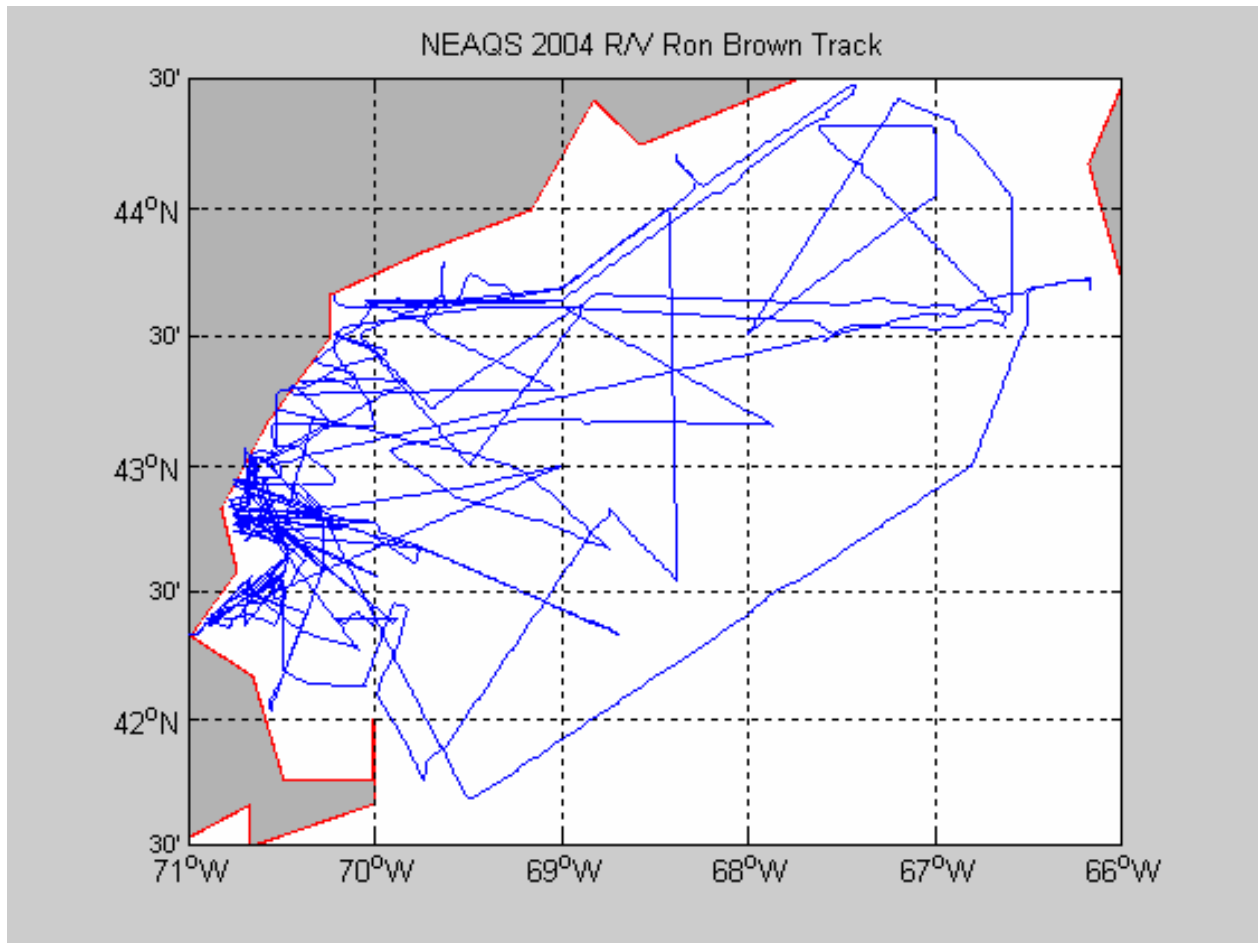


Figure 14. Cruise track for entire ICARTT/NEAQS 2004 cruise.

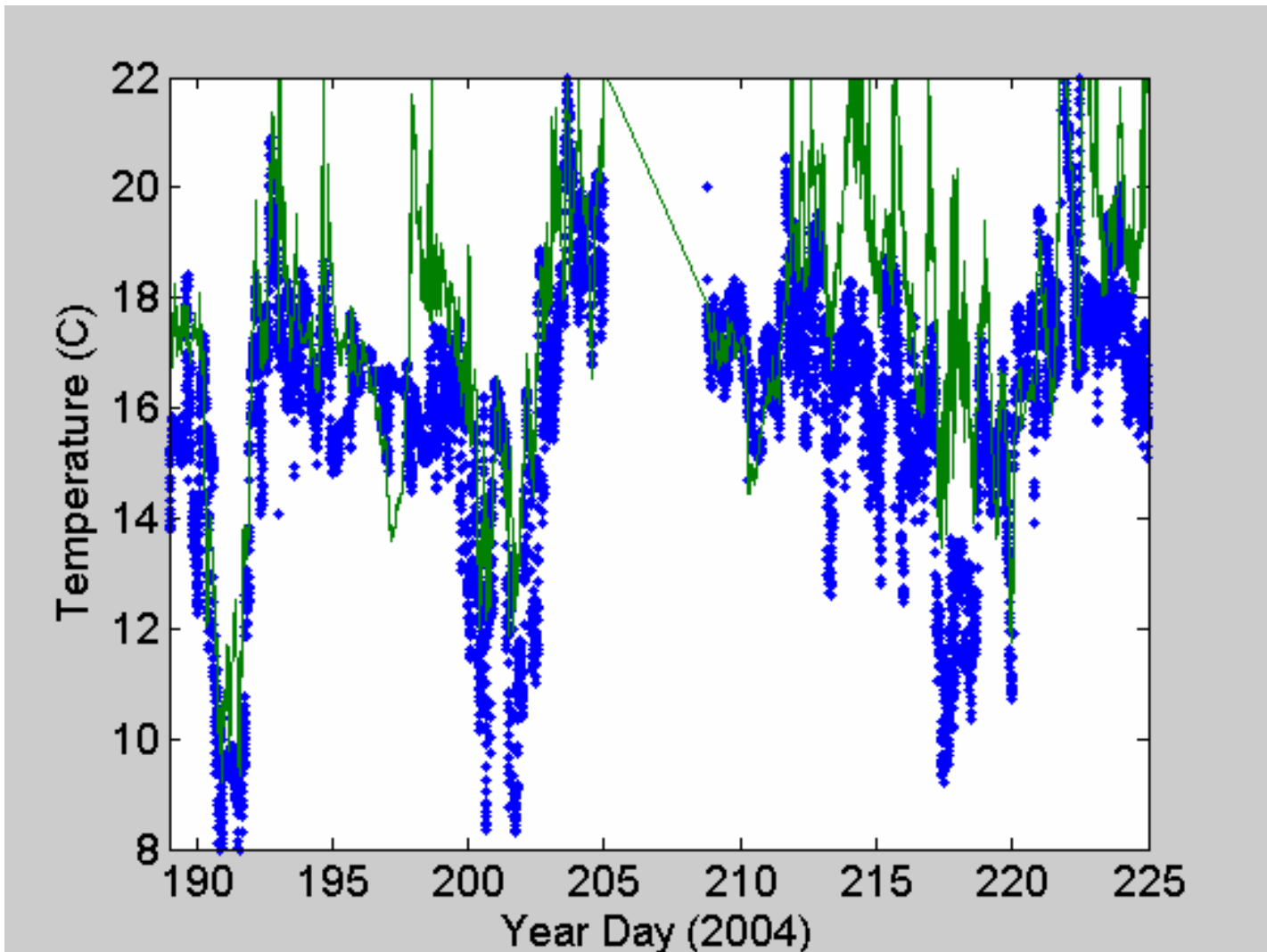


Figure 15. Time series of near-surface ocean temperature and 18-m air temperature for the 2004 RHB NEAQS cruise.

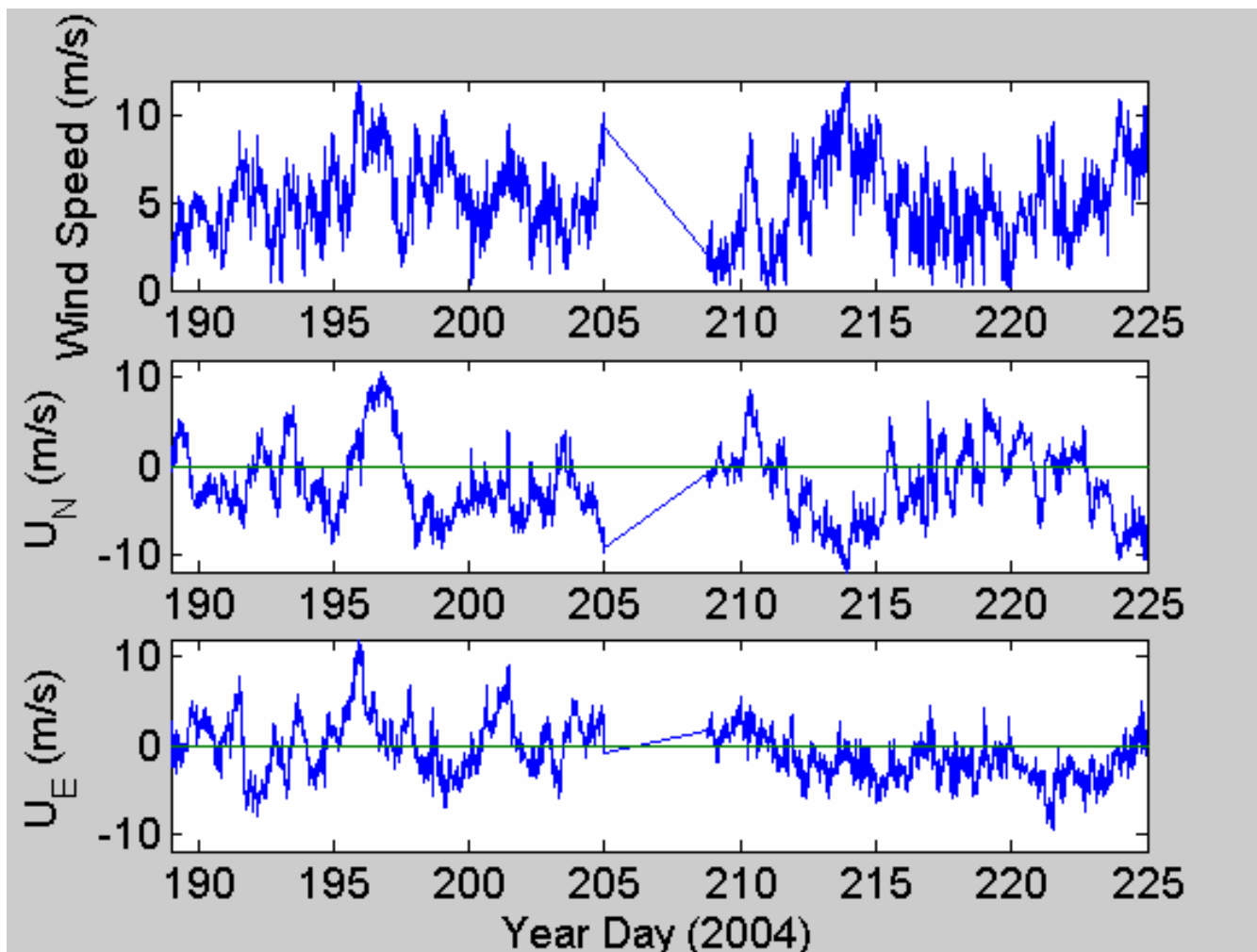


Figure 16. Time series of wind speed (upper panel), northerly component (middle panel), and easterly component (lower panel) for the 2004 RHB NEAQS cruise.

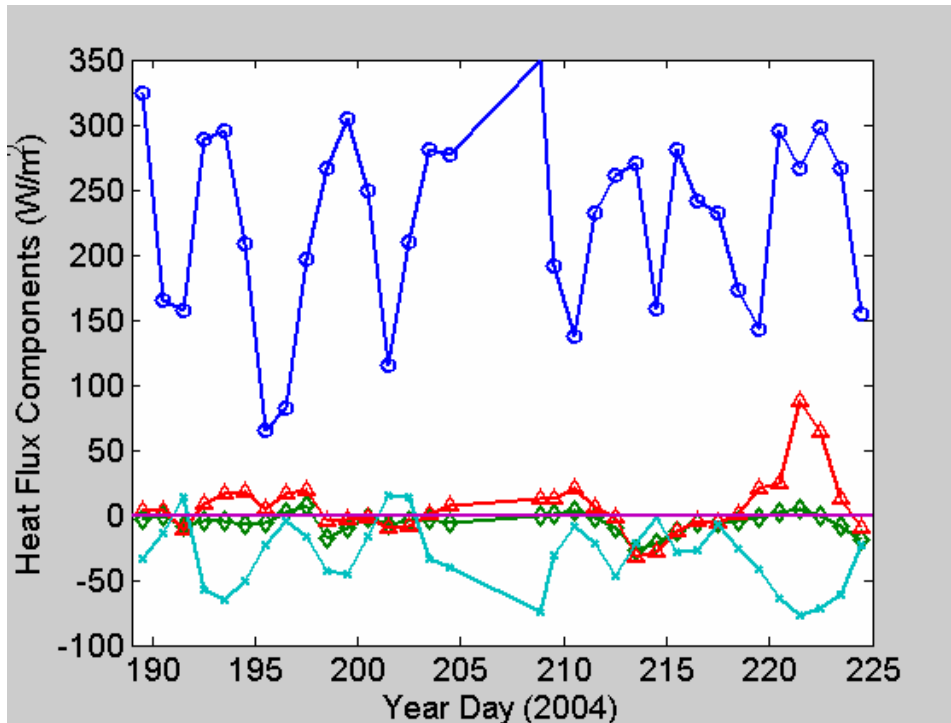


Figure 17. Time series of 24-hr average heat flux components: solar flux - circles; latent heat flux - triangles; sensible heat flux - diamonds; net IR flux x's.

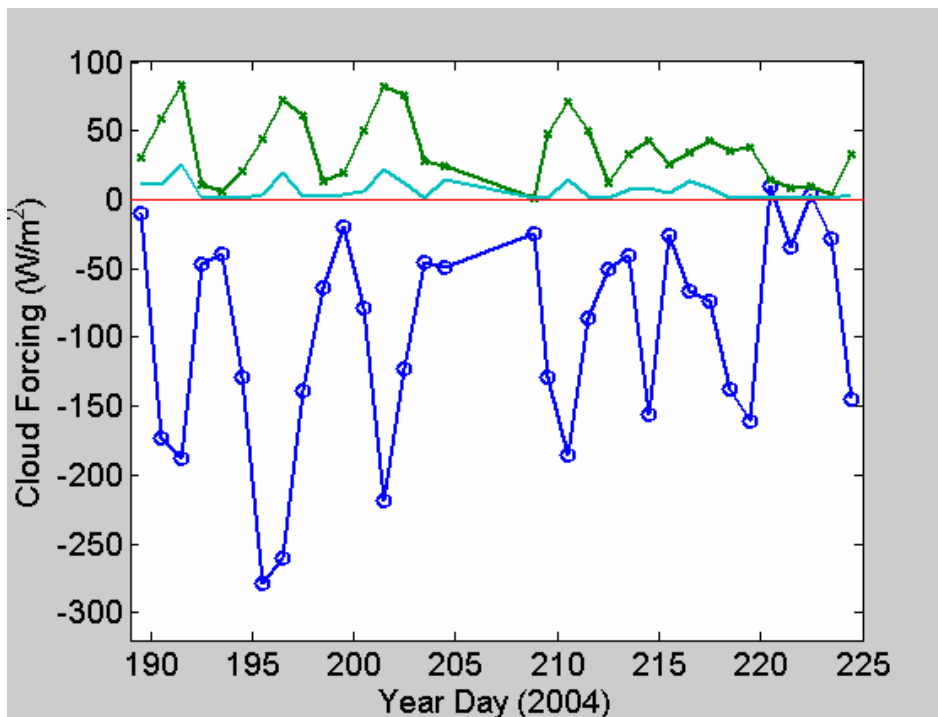


Figure 18. Time series of daily averaged radiative cloud forcing and precipitation: IR CF (W/m^2) – green, Solar CF (W/m^2) – blue, Rain rate (mm/day) - cyan.

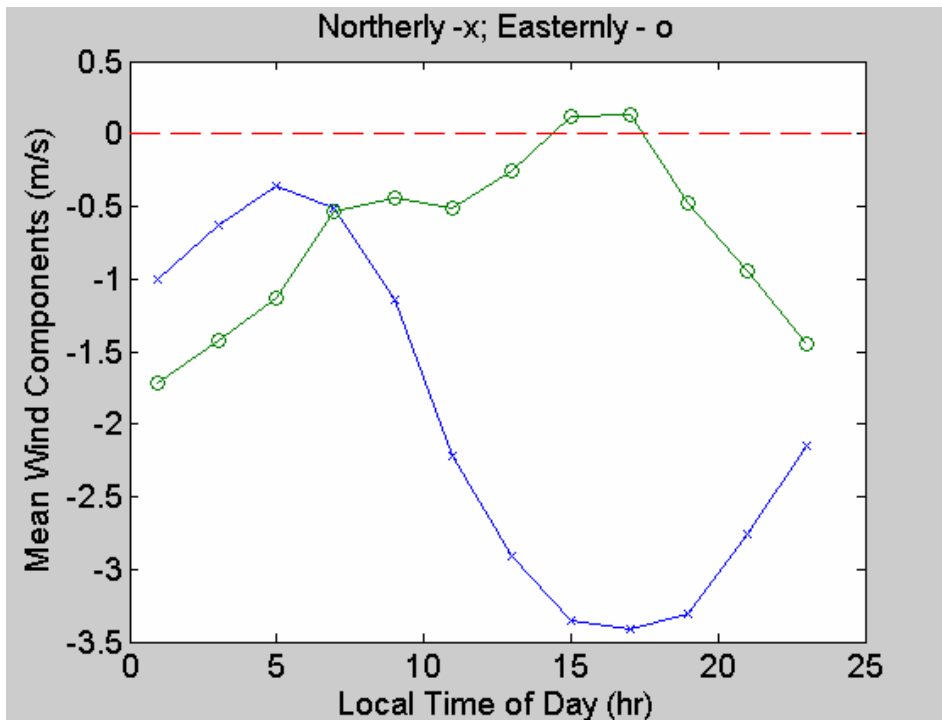


Figure 19. Diurnal average of northerly and easterly wind components for entire cruise.

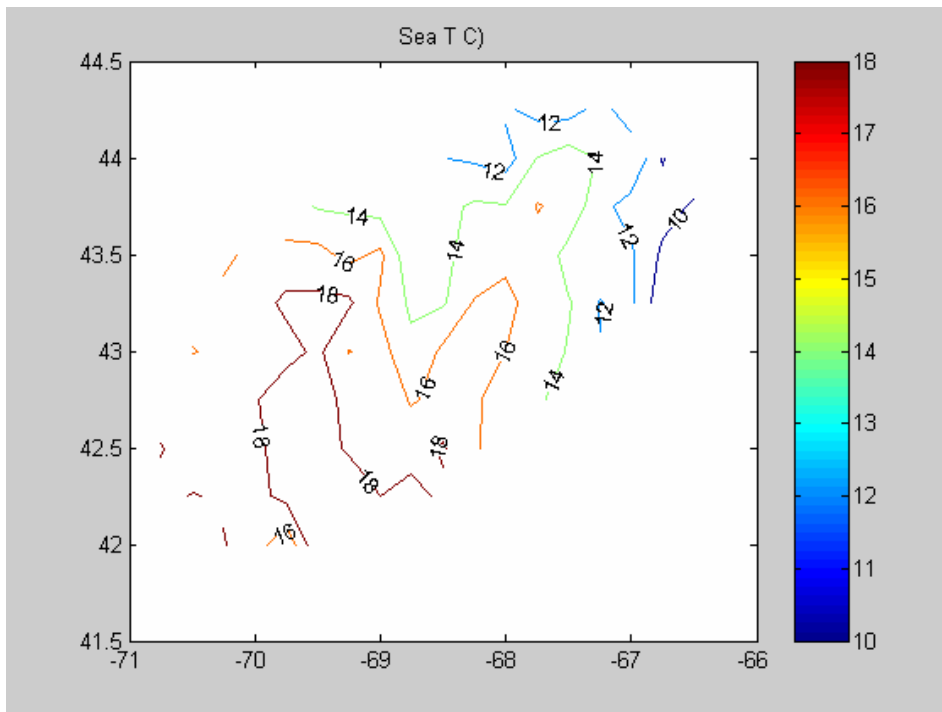


Figure 20. Contour map of ocean near-surface temperature (C.) from the ETL seasnake.

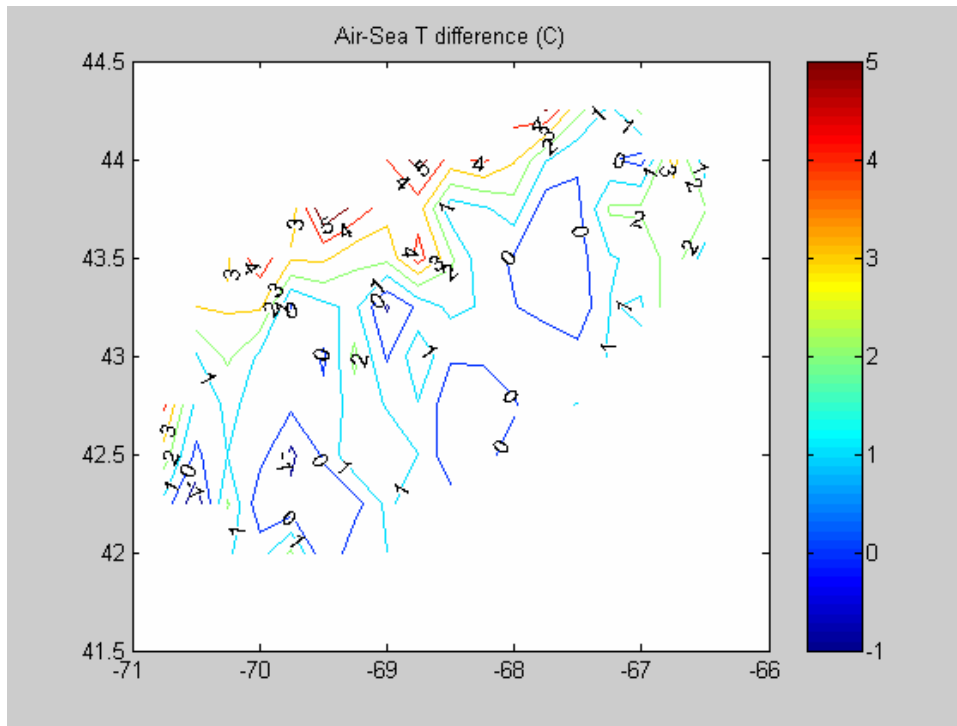


Figure 21. Contour map of air-sea temperature difference, $T_{air}-T_{sea}$ (C).

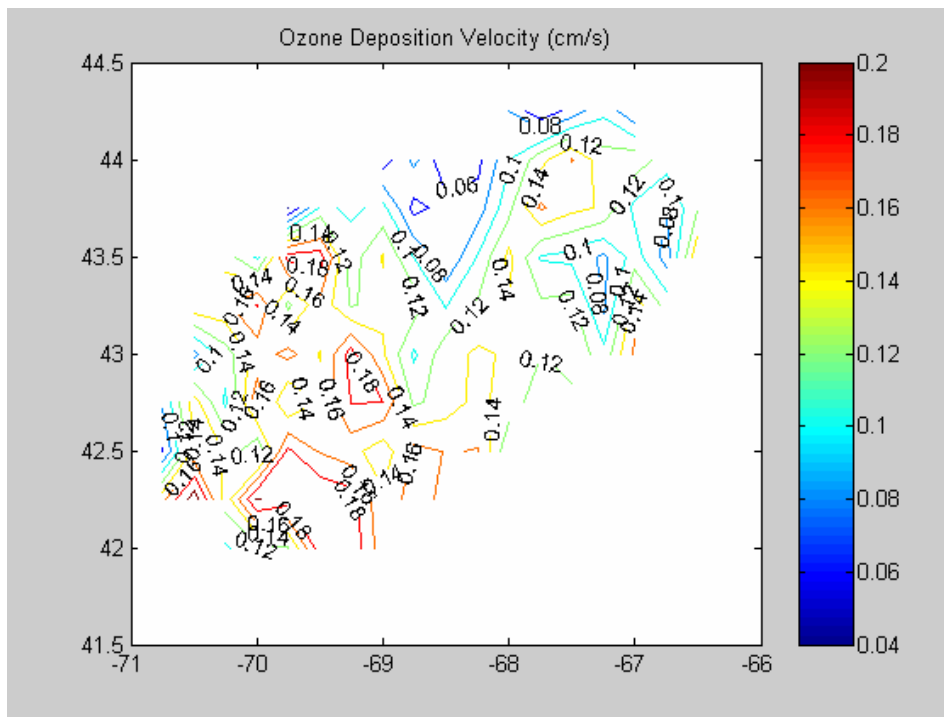


Figure 22. Contour map of ozone deposition velocity (cm/s) from the NOAA COARE gas transfer model.

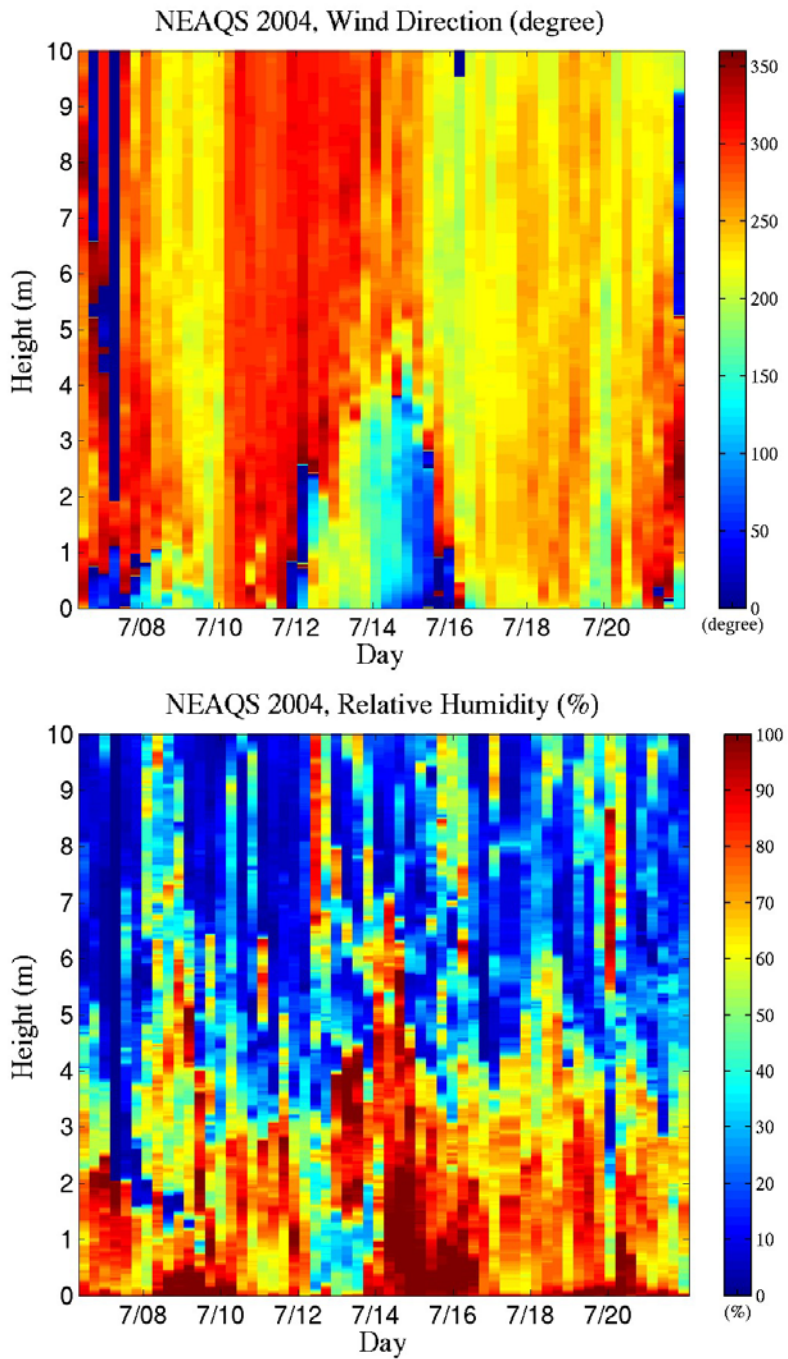


Figure 23. Time-height color contour plots from rawinsondes launched during the 2004 NEAQS cruise. The upper panel is wind direction; the lower panel is relative humidity.

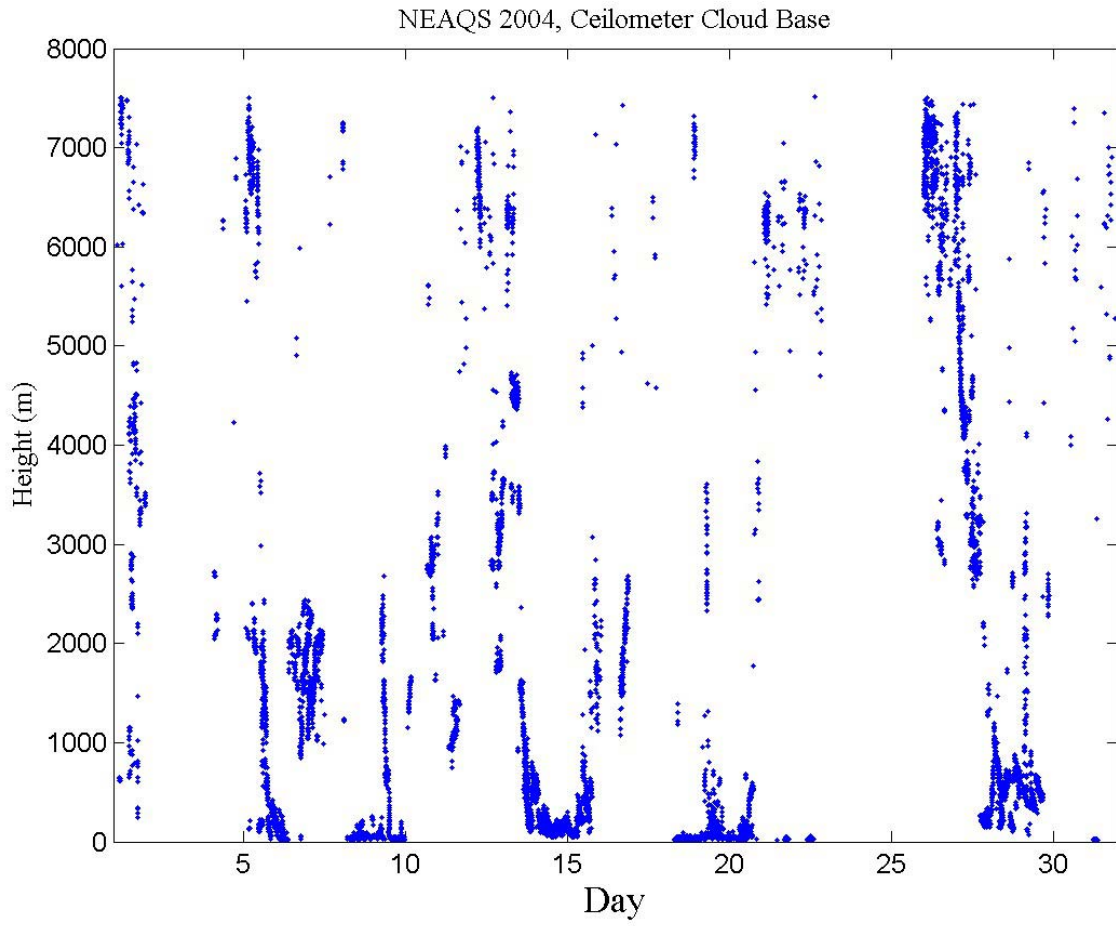


Figure 24. Time series of low cloud-base heights for the experimental period during July.